ACS APPLIED MATERIALS & INTERFACES

Letter

www.acsami.org

BiAg Alloy Nanospheres: A New Photocatalyst for H_2 Evolution from Water Splitting

Zhengbo Jiao,[†] Yan Zhang,[‡] Shuxin Ouyang,[§] Hongchao Yu,[†] Gongxuan Lu,[†] Jinhua Ye,[§] and Yingpu Bi*[,†]

[†]State Key Laboratory for Oxo Synthesis & Selective Oxidation, and National Engineering Research Center for Fine Petrochemical Intermediates, Lanzhou Institute of Chemical Physics, Chinese Academy of Science, Lanzhou 730000, China

[‡]College of Physics and Electronic Engineering, Northwest Normal University, Lanzhou 730000, China

[§]International Center for Materials Nanoarchitectonics, and Research Unit for Environmental Remediation Materials, National Institute for Materials Science, Tsukuba 305-0047, Japan

Supporting Information

ABSTRACT: We demonstrate for the first time that Bi and BiAg alloy nanospheres, fabricated with a facile hydrothermal method, display evident photocatalytic H_2 production activities. Element Bi can serve as an active photocatalyst for both water splitting and photoelectrochemical applications. More interestingly, these activities of Bi can be greatly enhanced by introducing Ag to form BiAg alloy nanoparticles, which may be ascribed to the improved charge separation and enlarged carrier concentration. The constituent of the BiAg alloy can be rationally tuned by varying the amount of Ag nanowires, and it is found that $Bi_{0.7}Ag_{0.3}$ exhibits the highest photoelectrochemical property.

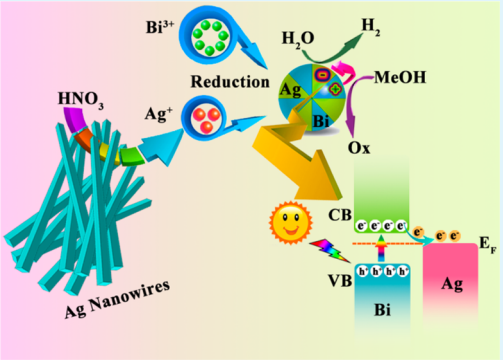

KEYWORDS: *photocatalysis, photoelectrochemical, H_2 evolution, BiAg alloy, nanospheres*

Photocatalytic H_2 evolution from water splitting, as a promising strategy to ease the energy crisis and environmental deterioration, has been attracting worldwide attention owing to its great significance in the sustainable development of human society.[1] Over the past decades, major efforts have been paid to compound semiconductors and little attention has been focused on elemental photocatalysts.[2,3] In recent years, elemental materials, such as P,[4] B,[5] Se,[6] and S,[7] have aroused people's recognition of photocatalysis because of their novel photocatalytic performances, suitable band edges for targeted reactions, good stability, and low cost. These developments not only represent the emergence of a new class of photocatalysts but also propel people to rediscover the essential principle of photocatalysis. Because of the limitation of the element quantity and the rigorous requirements for photocatalysis, the findings of semiconductors, especially elemental photocatalysts, are extremely difficult.[8,9] Moreover, the H_2 production from water splitting is more arduous for new photocatalysts because the conduction band edge must be negative enough for transmission of the photoexcited electrons to water.[10−13] This communication reports for the first time that element Bi can generate H_2 from water splitting and the introduction of Ag can significantly enhance its photocatalytic performance.[14−18] Besides the merits of elemental semiconductors described above, Bi and Ag are both heavy elements, which possess larger mass than nonmetal materials, and thus can be easily recycled by the precipitation method in their future practical applications.

Bi is a fascinating semimetal with a rhombohedral structure and a small energy overlap between the conduction and valence bands.[14,15] It has been extensively studied for its quantum transport, finite-size effect, and magnetoresistance effect.[16,17] Previous reports have predicted that, as the size decreases, Bi could achieve the transition from semimetal to semiconductor on the basis of quantum confinement.[18,19] Although various Bi nanostructures, including nanorods,[20] nanowires,[21] nanotubes,[22] nanoplates,[23] and nanospheres,[24,25] have been synthesized through different methods, their applications in photoelectrochemical and photocatalytic H_2 production have rarely been investigated until now. Herein, we demonstrate that metallic Bi nanospheres exhibit obvious water splitting activity. More importantly, element Ag can be successfully introduced to form BiAg alloy nanoparticles by the hydrothermal method using Ag nanowires as the Ag source. As expected, the photocatalytic H_2 production ability and photoelectric current of Bi can be significantly enhanced because of the improved charge separation and enlarged carrier concentration. Moreover, the content of Ag can be rationally tuned by varying the

Received: September 5, 2014
Accepted: November 7, 2014
Published: November 7, 2014

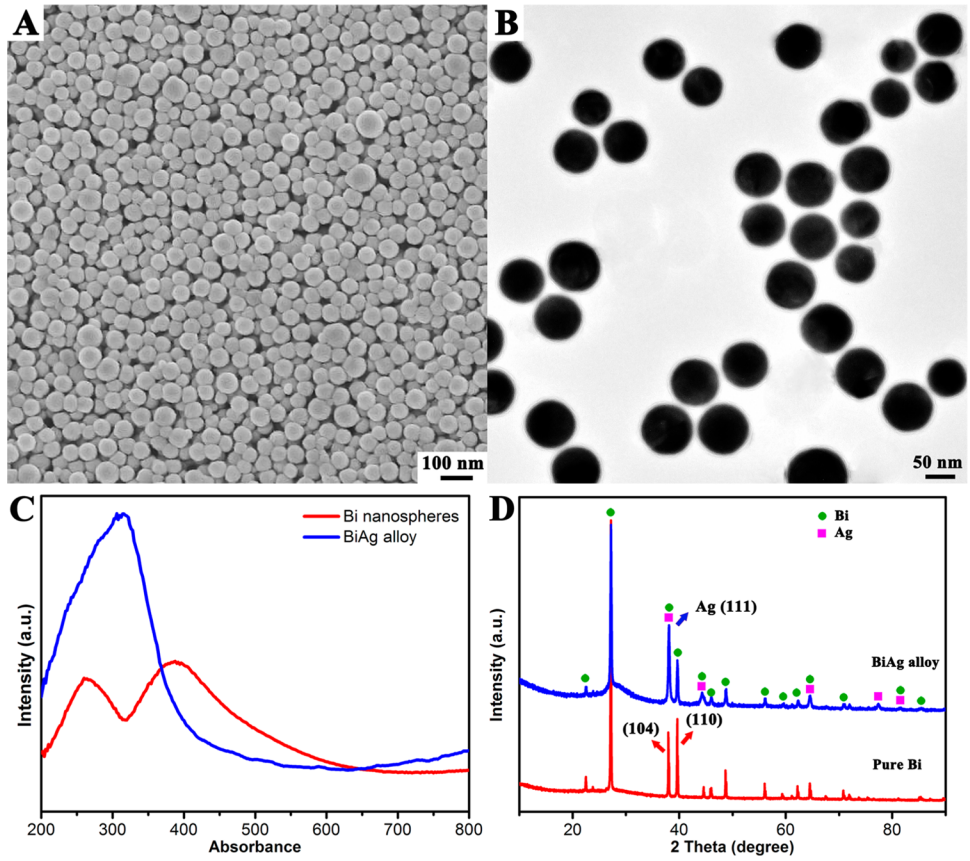

Figure 1. (A) SEM and (B) TEM images of BiAg alloy nanoparticles. (C) UV−vis diffusive-reflectance spectra. (D) XRD patterns of Bi and BiAg alloy nanospheres.

amount of Ag nanowires, and only the appropriate proportion can achieve the highest photocatalytic performance.

Single-crystalline Ag nanowires were first prepared through a modified polyol process and serve as the starting materials for the subsequent growth of BiAg alloy nanoparticles (Figures S1 and S2 in the Supporting Information, SI). At the beginning of the hydrothermal reaction, nitric acid would react with the as-prepared Ag nanowires to form Ag^+ ions. Then Ag^+ and Bi^{3+} would be reduced by ethylene glycol and aggregate together to form BiAg alloy nanoparticles. Here, it is worth noting that Ag nanowires play a double role during the hydrothermal process. On the one hand, it supplies the Ag source for the BiAg alloy, and, on the other hand, it controls the kinetics of the reaction. It is well-known that the redox potential of Ag species is +0.7996 V, which is much higher than that of Bi species (+0.308 V).[26] For this reason, it can be known that Ag^+ is more reductive than Bi^{3+}. Also, it can be rationally deduced that if Ag nanowires are replaced by Ag^+, such as $AgNO_3$, Ag ions will be reduced rapidly to form Ag nanoparticles but not the BiAg alloy. In addition, Ag nanowires are more stable than other morphologies, and they can release Ag ions leisurely during the 24 h hydrothermal reaction time. Therefore, we chose Ag nanowires as the Ag source. Ag nanowires must be first oxidized by nitric acid and then reduced by ethylene glycol, accompanying the reduction of Bi^{3+} ions. The reductive reaction rate could be conveniently controlled by the concentration of nitric acid, just as expressed by the following equation: $3Ag + 4HNO_3 \rightarrow 3AgNO_3 + NO + 2H_2O$.

Figure 1 presents the scanning electron microscopy (SEM) and transmission electron microscopy (TEM) images of BiAg alloy nanoparticles. It can be clearly seen that the morphology of BiAg nanospheres is generally uniform and their average dimension is about 52 nm. The surfaces of BiAg alloy nanospheres are smooth, and no secondary architectures are observed. Parts C and D of Figure 1 display the UV−vis diffusive-reflectance spectra and XRD patterns of Bi and BiAg alloy nanoparticles. It can be seen that Bi nanospheres are responsive to visible light and exhibit two absorption peaks, which center at 266 and 390 nm, respectively. It is believed that the first peak is regarded as the surface plasmon resonance of Bi and the second peak correlates with the dimension of nanoparticles.[15,19,27] It is worth noting that the edge of the absorbance peak of the BiAg alloy blue shifts reversely, which may be ascribed to the surface plasmon resonance of Ag centered at 320 nm (Figure S4 in the SI). The composition and crystal structure of Bi and BiAg alloy nanospheres have been further confirmed by XRD patterns, and the results are exhibited in Figure 1D. The XRD patterns of Bi nanoparticles are in good agreement with that of a pure rhombohedral Bi structure (JCPDS 44-1246; Figure S5 in the SI). It is interesting that most of the diffraction peaks of Ag are coincident with that of Bi except the one located at 77°, which may be a suitable reason for explaining why Bi and Ag can form alloy nanoparticles. In addition, it can be calculated that the intensity ratio of (104) to (110) of pure Bi is about 0.85, which is marked in Figure 1D. However, the relative value increased to 1.8 for the BiAg alloy because the highest (111) peak of Ag is overlapping with the (104) peak of Bi, which could further confirm the introduction of element Ag.

dx.doi.org/10.1021/am506030p | ACS Appl. Mater. Interfaces 2014, 6, 19488−19493

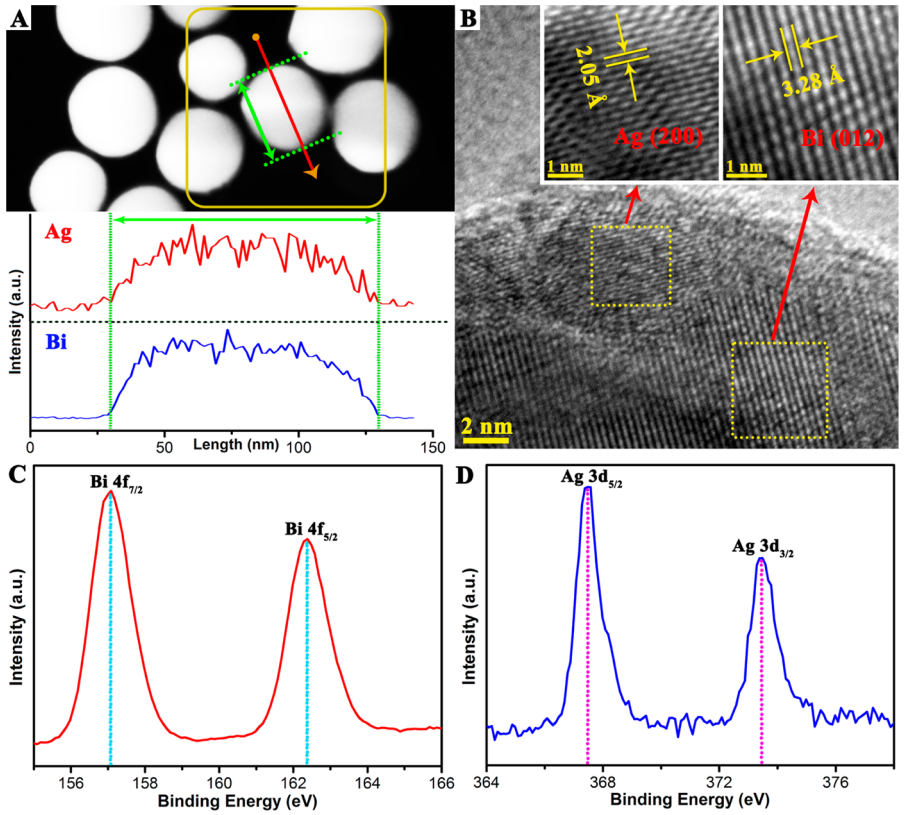

Figure 2. (A) EDS line analysis, (B) HRTEM image, and high-resolution (C) Bi 4f and (D) Ag 3d XPS spectra of BiAg alloy nanoparticles.

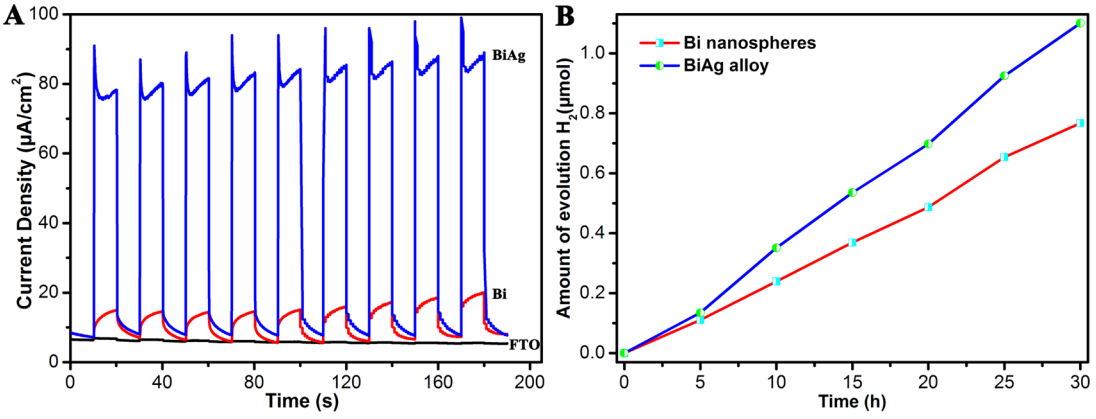

Figure 3. (A) Transient photocurrent densities measured with chopped light at 0.4 V vs SCE and (B) photocatalytic H_2 evolution from aqueous methanol solutions under UV–vis light irradiation over Bi and BiAg alloy nanoparticles.

In order to investigate the elemental distribution of Bi and Ag in the nanoparticles, energy-dispersive X-ray spectroscopy (EDS) line analysis of the BiAg alloy has been performed and is shown in Figure 2A. The red line over the span of 150 nm passes through a BiAg alloy nanosphere. It can be seen that the Bi and Ag elemental signals display obviously in the nanosphere area. In addition, the EDS elemental mapping spectra of four BiAg alloy nanoparticles were also carried out and are shown in Figure S6 in the SI. It can be concluded that the dispersion of elements Bi and Ag is homogeneous and uniform, indicating formation of the BiAg alloy. Besides, the amount of each element was detected by EDS (Figure S7 in the SI) and inductively coupled plasma optical emission spectrometry (Table S1 in the SI). It can be calculated that the molar ratio of Bi to Ag is about 7:3, and the value can be rationally tuned by varying the comparative amount of $Bi(NO_3)_3$ to that of Ag nanowires (Figure S8 and Table S1 in the SI). Moreover, to further clarify the concrete structure of the BiAg alloy and make clear the detailed conjunction manner between elements Bi and Ag, high-resolution TEM (HRTEM) was performed and is shown in Figure 2B. It can be distinctly observed that two different types of crystal lattices coexist in one nanosphere. One lattice fringe spacing is about 0.205 nm, corresponding to the (200) plane of Ag.[28] The other fringe spacing is around 0.328 nm, which is consistent with the (012) facet of Bi.[14] High-resolution X-ray photoelectron spectroscopy (XPS) of both Bi 4f and Ag 3d were examined to reveal their valence states, which are exhibited in parts C and D of Figure 2, respectively. The high-resolution spectrum of Bi 4f in Figure 2C demonstrates that the doublet peaks at 157.03 and 162.38 eV

dx.doi.org/10.1021/am506030p | ACS Appl. Mater. Interfaces 2014, 6, 19488–19493

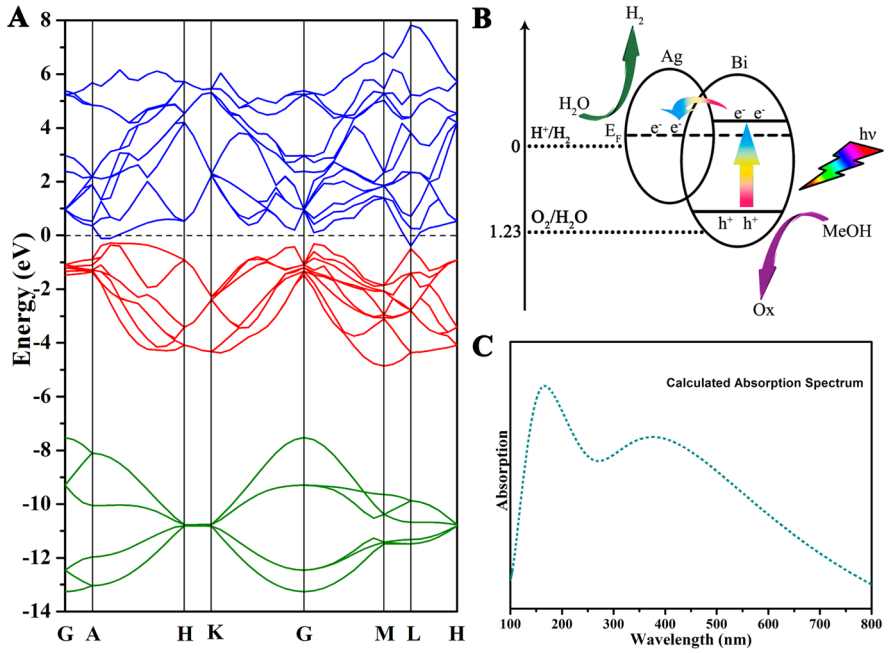

Figure 4. (A) Calculated energy band structure of Bi. (B) Schematic illustration for charge separation and migration in BiAg alloy nanoparticles. (C) Calculated electronic absorption spectrum of Bi.

can be assigned to Bi $4f_{7/2}$ and Bi $4f_{5/2}$, respectively, indicating that the splitting of the Bi 4f doublet is 5.35 eV.[29] Therefore, it can be deduced that element Bi remains metallic in nature. In the same way, it can be calculated from Ag $3d_{5/2}$ (367.48 eV) and Ag $3d_{3/2}$ (373.46 eV) that the splitting of the Ag 3d doublet is 5.98 eV, implying the zerovalent state of Ag (Figure 2D).[30] On the basis of the above results and discussion, it can be concluded that the nanoparticles are pure metallic BiAg alloy and no other impurities were introduced.

The photoelectrochemical performances and H_2 evolution activities of Bi and BiAg alloy nanoparticles were explored. For comparison, the photoelectrochemical property of pure FTO was also investigated. As shown in Figure 3A, the photocurrent density of Bi nanospheres can achieve 19 $\mu A/cm^2$, which is much higher than that of pure FTO. Therefore, it can be deduced that the photocurrent resulted from the separation of electron−hole pairs inside Bi nanospheres under light illumination. The photoelectrochemical activity of Bi can be greatly enhanced by introducing Ag to form the BiAg alloy, which may due to the lower Fermi level of Ag and the larger carrier concentration of the BiAg alloy. All BiAg alloy nanoparticles with different components exhibited much higher photocurrent density than pure Bi (Figure S9 in the SI). Also, when the molar ratio of Bi to Ag equals 7:3, the highest photoelectrochemical performance can be achieved. It can be seen that the photocurrent density of $Bi_{0.7}Ag_{0.3}$ reached 80 $\mu A/cm^2$, which is about 4 times larger than that of pure Bi. Thereby, it can be concluded that the optimal constituent is $Bi_{0.7}Ag_{0.3}$, and without special indications, the BiAg alloy in the text refers to this composition. In addition, a comparison of the XRD patterns of the BiAg alloy before and after photoelectrochemical experiments proves that they possess excellent stability (Figure S10 in the SI). The H_2 evolution performances of Bi and BiAg alloy nanoparticles have been examined and are shown in Figure 3B. Obviously, both Bi and BiAg alloy nanoparticles can split water to generate H_2, and the H_2 evolution rates of Bi and BiAg alloy nanoparticles are 0.022 and 0.036 μmol/h, respectively. Therefore, it can be deduced that the conduction band of Bi must be negative enough for transmission of the photoexcited electrons to water. Additionally, the H_2 production rate of BiAg alloy is also much higher than that of pure Bi nanospheres, which is consistent with their photoelectrochemical performances.

It is well-known that Bi is a typical semimetal with a small energy overlap between the conduction and valence bands.[14,15] The transition from semimetal to semiconductor is achieved with a decrease of the dimensions because of quantum confinement.[18,19] Thus, the electron−hole pairs inside the nanosized Bi particles may separate with the aid of external energy. In order to further make clear the mechanism of the photocatalytic properties of Bi, the energy band structure of element Bi was calculated by first-principles calculations, just as shown in Figure 4A. It can be observed that the valence energy band consists of two different parts. The area in the range of −13.3 to −7.5 eV is mainly composed of Bi 6s states, and the band between −5 and 0 eV is dominated by Bi 6p states. The empty conduction band, which is near the valence band and is illustrated by blue lines, is also composed of Bi 6p states. Under light illumination, electrons could be easily excited from the valence band to the conduction band and thus achieve separation of the holes, which can certify the prediction above. However, the photoexcited electrons may recombine with the holes rapidly owing to its metalloid property and the small energy gap. Therefore, the photoelectrochemical and photocatalytic performances of Bi are not outstanding. Nevertheless, it was discovered that these properties of Bi nanospheres could be greatly enhanced by introducing Ag to form BiAg alloy nanoparticles. It is known that the work function of Ag (4.26 eV) is higher than that of Bi (4.22 eV), indicating that the Fermi level of Ag is lower than that of Bi. Coupling Ag with Bi to form the BiAg alloy will lead to a new equilibrium Fermi level through the migration of electrons from Bi to Ag. It has been known that the conduction band of Bi is negative enough for water reduction. Therefore, under UV−vis

light illumination, the photogenerated electrons could be easily transferred from the conduction band of Bi to the surfaces of Ag (Figure 4B), which could significantly promote charge separation and thus enhance the photoelectrochemical as well as photocatalytic performances of Bi. In addition, the larger carrier concentration of the BiAg alloy (1.645×10^{20} cm^{-3}) over that of the Bi film (6.905×10^{11} cm^{-3}), which were determined using a Hall effect tester, may also contribute greatly to the improved photoelectrochemical activities. Besides, Figure 4C gives the calculated absorption spectrum of Bi on the basis of the energy band theory. It can be seen that the theoretical result is generally consistent with the experimental spectrum (Figure 1C). They both display obvious double-peak structure and visible-light absorption, which can indirectly prove the correctness of the energy band calculations.

In summary, it has been first discovered that element Bi exhibits obvious photocatalytic H_2 evolution performance from water splitting. More importantly, the photoelectrochemical and photocatalytic activities of Bi can be significantly enhanced by introducing Ag to form BiAg alloy nanoparticles, which may be ascribed to the improved photogenerated electron−hole pair separation and the enlarged carrier concentration. Additionally, it has been demonstrated that, during the production of BiAg alloy nanospheres, Ag nanowires instead of Ag ions should be used as the Ag source, and the constituent of the BiAg alloy can be rationally tuned by varying the amount of Ag nanowires. The photoelectrochemical properties of the BiAg alloy with different components have also been explored, and it is found that the optimal composition of the BiAg alloy is $Bi_{0.7}Ag_{0.3}$.

■ ASSOCIATED CONTENT

Supporting Information

Experimental details and additional figures and tables as mentioned in the text. This material is available free of charge via the Internet at http://pubs.acs.org.

■ AUTHOR INFORMATION

Corresponding Author

*E-mail: yingpubi@licp.cas.cn.

Notes

The authors declare no competing financial interest.

■ ACKNOWLEDGMENTS

This work was financially supported by the "Hundred Talents Program" of the Chinese Academy of Science and National Natural Science Foundation of China (Grants 21273255 and 21303232).

■ REFERENCES

(1) Yu, J.; Low, J.; Xiao, W.; Zhou, P.; Jaroniec, M. Enhanced Photocatalytic CO_2-Reduction Activity of Anatase TiO_2 by Coexposed {001} and {101} Facets. *J. Am. Chem. Soc.* **2014**, *136*, 8839−8842.

(2) Luo, W.; Yang, Z.; Li, Z.; Zhang, J.; Liu, J.; Zhao, Z.; Wang, Z.; Yan, S.; Yu, T.; Zou, Z. Solar Hydrogen Generation from Seawater with a Modified $BiVO_4$ Photoanode. *Energy Environ. Sci.* **2011**, *4*, 4046−4051.

(3) Bi, Y.; Ouyang, S.; Umezawa, N.; Cao, J.; Ye, J. Facet Effect of Single-Crystalline Ag_3PO_4 Sub-microcrystals on Photocatalytic Properties. *J. Am. Chem. Soc.* **2011**, *133*, 6490−6492.

(4) Wang, F.; Ng, W. K. H.; Yu, J. C.; Zhu, H.; Li, C.; Zhang, L.; Liu, Z.; Li, Q. Red Phosphorus: An Elemental Photocatalyst for Hydrogen Formation from Water. *Appl. Catal., B* **2012**, *111−112*, 409−414.

(5) Liu, G.; Yin, L. C.; Niu, P.; Jiao, W.; Cheng, H. M. Visible-Light-Responsive β-Rhombohedral Boron Photocatalysts. *Angew. Chem., Int. Ed.* **2013**, *125*, 6362−6365.

(6) Chiou, Y. D.; Hsu, Y. J. Room-temperature Synthesis of Single-crystalline Se Nanorods with Remarkable Photocatalytic Properties. *Appl. Catal., B* **2011**, *105*, 211−219.

(7) Liu, G.; Niu, P.; Yin, L.; Cheng, H. M. α-Sulfur Crystals as a Visible-Light-Active Photocatalyst. *J. Am. Chem. Soc.* **2012**, *134*, 9070−9073.

(8) Yerga, R. M. N.; Galván, M. C. Á.; Valle, F.; Mano, J. V.; Fierro, J. L. G. Water Splitting on Semiconductor Catalysts under Visible-light Irradiation. *ChemSusChem* **2009**, *2*, 471−485.

(9) Zhu, J.; Zäch, M. Nanostructured Materials for Photocatalytic Hydrogen Production. *Curr. Opin. Colloid Interface Sci.* **2009**, *14*, 260−269.

(10) Mukherji, A.; Seger, B.; Lu, G. Q.; Wang, L. Z. Nitrogen Doped $Sr_2Ta_2O_7$ Coupled with Graphene Sheets as Photocatalysts for Increased Photocatalytic Hydrogen Production. *ACS Nano* **2011**, *5*, 3483−3492.

(11) Zhang, P.; Zhang, J.; Gong, J. Tantalum-based Semiconductors for Solar Water Splitting. *Chem. Soc. Rev.* **2014**, *43*, 4395−4422.

(12) Jorge, A. B.; Martin, D. J.; Dhanoa, M. T. S.; Rahman, A. S.; Makwana, N.; Tang, J.; Sella, A.; Cora, F.; Firth, S.; Darr, J. A.; McMillan, P. F. H_2 and O_2 Evolution from Water Half-Splitting Reactions by Graphitic Carbon Nitride Materials. *J. Phys. Chem. C* **2013**, *117*, 7178−7185.

(13) Shang, L.; Zhou, C.; Bian, T.; Yu, H.; Wu, L. Z.; Tung, C. H.; Zhang, T. Facile Synthesis of Hierarchical $ZnIn_2S_4$ Submicrospheres Composed of Ultrathin Mesoporous Nanosheets as a Highly Efficient Visible-Light-Driven Photocatalyst for H_2 Production. *J. Mater. Chem. A* **2013**, *1*, 4552−4558.

(14) Wang, W. Z.; Poudel, B.; Ma, Y.; Ren, Z. F. Shape Control of Single Crystalline Bismuth Nanostructures. *J. Phys. Chem. B* **2006**, *110*, 25702−25706.

(15) Wang, Y. W.; Hong, B. H.; Kim, K. S. Size Control of Semimetal Bismuth Nanoparticles and the UV−Visible and IR Absorption Spectra. *J. Phys. Chem. B* **2005**, *109*, 7067−7072.

(16) Yang, F. Y.; Liu, K.; Hong, K.; Reich, D. H.; Searson, P. C.; Chien, C. L. Large Magnetoresistance of Electrodeposited Single-Crystal Bismuth Thin Films. *Science* **1999**, *284*, 1335−1337.

(17) Liu, H.; Wang, Z. L. Bismuth Spheres Grown in Self-Nested Cavities in a Silicon Wafer. *J. Am. Chem. Soc.* **2005**, *127*, 15322−15326.

(18) Boukai, A.; Xu, K.; Heath, J. R. Size-Dependent Transport and Thermoelectric Properties of Individual Polycrystalline Bismuth Nanowires. *Adv. Mater.* **2006**, *18*, 864−869.

(19) Wang, Y.; Chen, J.; Chen, L.; Chen, Y. B.; Wu, L. M. Shape-Controlled Solventless Syntheses of Nano Bi Disks and Spheres. *Cryst. Growth Des.* **2010**, *10*, 1578−1584.

(20) Reppert, J.; Rao, R.; Skove, M.; He, J.; Craps, M.; Tritt, T.; Rao, A. M. Laser-assisted Synthesis and Optical Properties of Bismuth Nanorods. *Chem. Phys. Lett.* **2007**, *442*, 334−338.

(21) Gibbons, Y. H.; Buhro, W. E. Bismuth, Tellurium, and Bismuth Telluride Nanowires. *J. Mater. Chem.* **2004**, *14*, 595−602.

(22) Li, Y.; Wang, J.; Deng, Z.; Wu, Y.; Sun, X.; Yu, D.; Yang, P. Bismuth Nanotubes: A Rational Low-Temperature Synthetic Route. *J. Am. Chem. Soc.* **2001**, *123*, 9904−9905.

(23) Fu, R.; Xu, S.; Lu, Y. N.; Zhu, J. J. Synthesis and Characterization of Triangular Bismuth Nanoplates. *Cryst. Growth Des.* **2005**, *5*, 1379−1385.

(24) Wang, J.; Wang, X.; Peng, Q.; Li, Y. Synthesis and Characterization of Bismuth Single-Crystalline Nanowires and Nanospheres. *Inorg. Chem.* **2004**, *43*, 7552−7556.

(25) Wang, Y.; Xia, Y. Bottom-Up and Top-Down Approaches to the Synthesis of Monodispersed Spherical Colloids of Low Melting-Point Metals. *Nano Lett.* **2004**, *4*, 2047−2050.

(26) Xiong, J.; Jiao, Z.; Lu, G.; Ren, W.; Ye, J.; Bi, Y. Facile and Rapid Oxidation Fabrication of BiOCl Hierarchical Nanostructures with Enhanced Photocatalytic Properties. *Chem.—Eur. J.* **2013**, *19*, 9472−9475.

(27) Wang, Y.; Ibisate, M.; Li, Z. Y.; Xia, Y. Metallodielectric Photonic Crystals Assembled from Monodisperse Spherical Colloids of Bismuth and Lead. *Adv. Mater.* **2006**, *18*, 471−476.
(28) Zeng, J.; Zheng, Y.; Rycenga, M.; Tao, J.; Li, Z. Y.; Zhang, Q.; Zhu, Y.; Xia, Y. Controlling the Shapes of Silver Nanocrystals with Different Capping Agents. *J. Am. Chem. Soc.* **2010**, *132*, 8552−8553.
(29) Hamm, U. W.; Kramer, D.; Zhai, R. S.; Kolb, D. M. On the Valence State of Bismuth Adsorbed on a Pt (111) Electrode: An Electrochemistry, LEED and XPS Study. *Electrochem. Acta* **1998**, *43*, 2969−2978.
(30) Zhang, G.; Keita, B.; Dolbecq, A.; Mialane, P.; Sécheresse, F.; Miserque, F.; Nadjo, L. Green Chemistry-Type One-Step Synthesis of Silver Nanostructures Based on Mo^{V}−Mo^{VI} Mixed-Valence Polyoxometalates. *Chem. Mater.* **2007**, *19*, 5821−5823.